Short-Range Order in Amorphous and Crystalline Ferroelectric Hf0.5Zr0.5O2

Erenburg, S. B.; Trubina, S. V.; Kvashnina, K. O.; Kruchinin, V. N.; Gritsenko, V. V.; Chernikova, A. G.; Markeev, A. M.;

Perma-Link to Publication Repository of HZDR:

https://www.hzdr.de/publications/Publ-27841

Short-Range Order in Amorphous and Crystalline Ferroelectric $Hf_{0.5}Zr_{0.5}O_2$

S. B. Erenburg[a,b,*], S. V. Trubina[a,**], K. O. Kvashnina[c,d], V. N. Kruchinin[e],
V. V. Gritsenko[e,f,g], A. G. Chernikova[h], and A. M. Markeev[h]

[a] *Institute of Inorganic Chemistry, Siberian Branch, Russian Academy of Sciences, Novosibirsk, 630090 Russia*
[b] *Institute of Nuclear Physics, Siberian Branch, Russian Academy of Sciences, Novosibirsk, 630090 Russia*
[c] *ESRF, Grenoble, 38043 France*
[d] *HZDR, Institute of Resource Ecology, Dresden, 01314 Germany*
[e] *Institute of Semiconductor Physics, Siberian Branch,*
Russian Academy of Sciences, Novosibirsk, 630090 Russia
[f] *Novosibirsk State University, Novosibirsk, 630090 Russia*
[g] *Novosibirsk State Technical University, Novosibirsk, 630073 Russia*
[h] *Moscow Institute of Physics and Technology, Dolgoprudnyi, Moscow oblast, 141700 Russia*

*e-mail: simon@niic.nsc.ru
**e-mail: svt@niic.nsc.ru

Abstract—The microstructures of amorphous and polycrystalline ferroelectric $Hf_{0.5}Zr_{0.5}O_2$ films are studied by X-ray spectroscopy and ellipsometry. EXAFS spectra demonstrate that the amorphous film consists of an "incompletely mixed" solid solution of metallic oxides HfO_2 and ZrO_2. After rapid thermal annealing, the mixed $Hf_{0.5}Zr_{0.5}O_2$ oxide films have a more ordered polycrystalline structure, and individual Hf and Zr monoxide islands form in the films. These islands are several nanometers in size and have a structure that is similar to the monoclinic structure of HfO_2 and ZrO_2. The presence of the HfO_2 and ZrO_2 phases in the $Hf_{0.5}Zr_{0.5}O_2$ films is also detected by ellipsometry.

1. INTRODUCTION

The authors of [1, 2] were the first to discover the ferroelectric effect in hafnium oxide, which was considered to be a paraelectric material over more than one hundred years. This effect was revealed in thin 10-nm-thick films doped by various elements, including Si, Al, Y, Gd, and Lz, and then annealed at a high temperature (about 1000°C). The fact that the ferroelectric effect was also detected in polycrystalline thin films of an $Hf_{0.5}Zr_{0.5}O_2$ solid solution not subjected to high-temperature annealing is of particular interest [3−7]. The appearance of ferroelectricity in these materials was related to the orthorhombic $Pbc2_1$ phase stabilized in them [3]. It is important that hafnium oxide−based materials have a number of advantages over traditional ferroelectrics: they are compatible with traditional modern microelectronic processes and have demonstrated their abilities to provide a very high element density. Due to the well-known advantages of ferroelectric random access memory (FeRAM), such as nonvolatile memory, high-speed performance, and a large number of switching cycles (more than 10^{10}), the discovery of ferroelectricity in such materials revives the concept of universal memory, which can cause a substantial breakthrough in the development of silicon devices [8].

The hafnium and zirconium atoms in cubic HfO_2 and tetragonal ZrO_2 (space group $Fm3m$ (no. 225) and $P4_2/nmc$ (no. 137), respectively) are coordinated by eight oxygen atoms; that is, these phases consist of HfO_8 and ZrO_8 structural units [9]. The oxygen atoms in these phases are coordinated by four hafnium and zirconium atoms. The hafnium and zirconium atoms in monoclinic HfO_2 and orthorhombic ZrO_2 (space group $P2_1/c$ (no. 14) and $Pbca$ (no. 61), respectively) are coordinated by seven oxygen atoms; that is, these phases consist of HfO_7 and ZrO_7 structural units [10]. Half the oxygen atoms in these phases are coordinated by four Hf and Zr atoms, and the remaining oxygen atoms, by three Hf and Zr atoms.

In the general case, the structure of the binary $Hf_{0.5}Zr_{0.5}O_2$ compound can be described by the random mixture (RM) or the random bonding (RB) model [11, 12]. In the RM model, orthorhombic

$Hf_{0.5}Zr_{0.5}O_2$ is represented by a mixture of HfO_2 and ZrO_2, which consist of HfO_7 and ZrO_7 structural units. In the RB model, $Hf_{0.5}Zr_{0.5}O_2$ consists of structural units HfO_vZr_{7-v}, $v = 0, 1, 2, 3, 4, 5, 6,$ and 7, where zirconium atoms statistically substitute for oxygen atoms in the HfO_7 structural unit. The purpose of this work is to study the structure of amorphous and polycrystalline ferroelectric $Hf_{0.5}Zr_{0.5}O_2$ by EXAFS (extended X-ray absorption fine structure) spectroscopy and ellipsometry using the effective-medium theory and to choose between the RM and RB structural models.

2. Structure Synthesis

The synthesized samples to be studied consisted of semiconductor−insulator, $Si/Hf_{0.5}Zr_{0.5}O_2$, structures. 10-nm-thick $Hf_{0.5}Zr_{0.5}O_2$ films were grown by atomic layer deposition at a temperature of 240°C using precursors $Hf[N(CH_3)(C_2H_5)]_4$ (TEMAH) and $Zr[N(CH_3)(C_2H_5)]_4$ (TEMAZ) and the H_2O oxidizer. TEMAH and TEMAZ precursors were preliminarily stirred to form a mixture. $Hf_{0.5}Zr_{0.5}O_2$ films were deposited onto n-type Si(100) wafers. The $Hf_{0.5}Zr_{0.5}O_2$ film thickness and stoichiometry were controlled by laser ellipsometry and Rutherford backscattering spectroscopy. Some samples were subjected to rapid thermal annealing (RTA) at 400°C for 30 s in an N_2 atmosphere. X-ray diffraction (XRD) studies of the deposited films without annealing and after RTA were performed on an ARL X'TRA (Thermo Scientific) powder diffractometer using CuK_α radiation and the Bragg−Brentano scheme. The $Hf_{0.5}Zr_{0.5}O_2$ films were amorphous after synthesis and became polycrystalline after RTA.

XRD analysis of the grown $Hf_{0.5}Zr_{0.5}O_2$ film after RTA demonstrated a number of intense lines, which indicated the formation of a polycrystalline structure consisting of the monoclinic, tetragonal, and orthorhombic ($Pbc2_1$) phases [13]. Note that the orthorhombic phase is responsible for the appearance of ferroelectricity in $Hf_{0.5}Zr_{0.5}O_2$ [3].

3. EXPERIMENTAL

3.1. EXAFS Measurement Technique

The EXAFS spectra of the amorphous and polycrystalline $Hf_{0.5}Zr_{0.5}O_2$ films were measured at the BM20 station, ESRF, Grenoble, France. Plates with ferroelectric films were glued to a table and placed under a monochromatic synchrotron radiation beam at an angle of about 1°. The spectra were measured at (i) absorption edge ZrK in the energy range 17753–18748 eV, which corresponds to the wavenumber k range up to 14 Å^{-1} (X-ray absorption edge ZrK is 17998 eV) and (ii) absorption edge HfL_1 in the energy range 11026−12021 eV, which corresponds to the k range up to 14 Å^{-1} (X-ray absorption edge HfL_1 is 11271 eV).

The spectra were measured under fluorescence conditions with a 12-channel Ge detector. Si(111) was used as a crystal−monochromator. Two mirrors with an Rh coating were used to focus a beam in the horizontal and vertical planes. The quantum flux in recording spectra was approximately 3×10^{11} photons/s in a beam 200 μm × 5 mm in size. Three scans were recorded for each sample and the best one was then chosen.

3.2. Processing and Simulation of EXAFS Spectra

It should be noted that the signal-to-noise ratio in the spectra of the samples is rather low. After 10 Å^{-1}, reliable EXAFS modulations are very weak in all spectra (even for stoichiometric oxides), which points to structural disordering in the films (which is likely to be represented by an amorphous structure, the presence of several phases, nonstoichiometry, vacancies). Therefore, we used experimental $\chi(k)$ EXAFS functions with weighting factor k taken in the first order, i.e., $k\chi(k)$, for simulation in some cases.

The EXAFS spectra of $Hf_{0.5}Zr_{0.5}O_2$ were simulated with the EXCURVE software package in the wavenumber range $k = 3.0−11.0$ Å^{-1} [14]. Simulation was carried out for both R-space-filtered ($\Delta R = 1−4$ Å^{-1} for HfL_1 spectra and $\Delta R = 0.8−4.1$ Å^{-1} for ZrK spectra) and unfiltered (initial) EXAFS spectra. Amplitude suppression factor S_0^2, which takes into account the photoionization-induced multielectron processes, was taken to be 0.7 in simulating ZrK spectra (parameter was obtained in simulating the reference ZrO_2 oxide) and 0.9 in simulating HfL_1 spectra (parameter was obtained in simulating the reference HfO_2 oxide). The Debye−Waller factors were separately calculated for the coordination shells of oxygen and a metal (Hf, Zr).

In the case of binary oxides, we were able to simulate spectra only for polycrystalline samples for EXAFS ZrK spectra. The local-structure parameters were determined in the k space ($\Delta k = 3−10$ Å^{-1}) for the unfiltered (initial) spectrum. In this case, the fitting of an unfiltered spectrum gives a smaller simulation error than that of an R-space-filtered spectrum (apparently, because of wider spikes (deviations) in a spectrum, which can yield ghost peaks during Fourier transform).

3.3. Ellipsometric Measurement Technique

The optical characteristics (refractive index $n(\lambda)$, absorption coefficient $k(\lambda)$) and the thickness of the ZrO_2, HfO_2, and $Hf_{0.5}Zr_{0.5}O_2$ films were determined with a Spektroskan ellipsometer. The dependences of
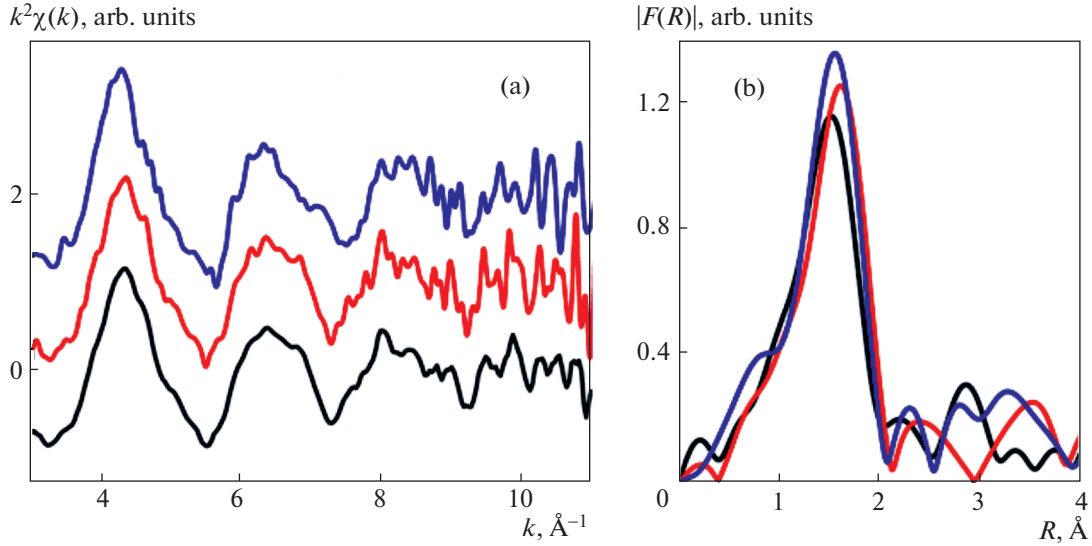
Fig. 1. (Color online) (a) Experimental HfL_1 EXAFS spectra and (b) moduli of their Fourier transform for films (back line) HfO$_2$, (red line) amorphous Hf$_{0.5}$Zr$_{0.5}$O$_2$, and (blue line) polycrystalline Hf$_{0.5}$Zr$_{0.5}$O$_2$.

ellipsometric angles ψ and Δ were measured in the wavelength range 250–1000 nm. The spectral resolution of the device was 2 nm, the spectrum recording time did not exceed 20 s, and the angle of beam incidence was 70°™. Four zones were measured and the measurement results were zone-averaged.

3.4. Processing and Simulation of Ellipsometric Spectral Measurements

The solution of the inverse problem of ellipsometry and the fitting of the spectral dependences of ellipsometric angles Ψ(λ) and Δ(λ) were performed according to the basic ellipsometry equation

$$\tan \Psi e^{i\Delta} = \frac{R_p}{R_s}, \qquad (1)$$

where R_p and R_s are the complex reflection coefficients for the waves polarized in the plane of incidence and normal to it. These coefficients depend on the optical constants and the layer thicknesses. To calculate the dispersion dependences of refractive index $n(\lambda)$ and absorption coefficient $k(\lambda)$ of a film and its thickness d, we used the following optical model of a single-layer reflecting system: isotropic substrate–isotropic homogeneous film–medium. The spectral dependences of polarization angles Ψ and Δ over the entire spectral range were independently fitted for each of the m spectral points by minimizing the error function

$$\sigma^2 = \frac{1}{2m - n - 1}$$
$$\times \sum_{i=1}^{m} [|\Delta_{exp}^i - \Delta_{calc}^i| + |\Psi_{exp}^i - \Psi_{calc}^i|], \qquad (2)$$

where Ψ$_{exp}$, Δ$_{exp}$ and Ψ$_{calc}$, Δ$_{calc}$ are the experimental and calculated ellipsometric parameters, respectively; m is the number of points in the spectrum; and n is the number of the desired parameters during calculation.

The dispersion dependence of the refractive index $n(\lambda)$ for the HfO$_2$, ZrO$_2$, and Hf$_{0.5}$Zr$_{0.5}$O$_2$ films that are transparent in the optical region under study is described by the polynomial Cauchy relation [15]

$$n(\lambda) = a + \frac{b}{\lambda^2} + \frac{c}{\lambda^4}, \qquad (3)$$

where a, b, and c are coefficients.

To calculate the dispersion dependences of the refractive index ($n(E)$) and the absorption coefficient ($k(E)$) of complex binary oxide films, we used the Bruggemann effective-medium model [15–17]

$$\sum_{i} \left(q_i \frac{\varepsilon_i - \varepsilon_{eff}}{\varepsilon_i + 2\varepsilon_{eff}} \right) = 0, \qquad (4)$$

where ε_i and ε_{eff} are the complex permittivities ($\varepsilon = N^2 = (n - ik)^2$) of the ith mixture component and the effective medium, respectively.

RESULTS AND DISCUSSION

4.1. EXAFS and XANES Spectra

Figures 1 and 2 show the experimental HfL_1 and ZrK spectra, respectively.

4.1.1. Results of simulation of the stoichiometric HfO$_2$ and ZrO$_2$ oxides. When simulating the stoichiometric HfO$_2$ and ZrO$_2$ oxides, we fixed the average coordination numbers in the shells of oxygen, hafnium, and zirconium according to the crystallographic data for the monoclinic structure [18], and the
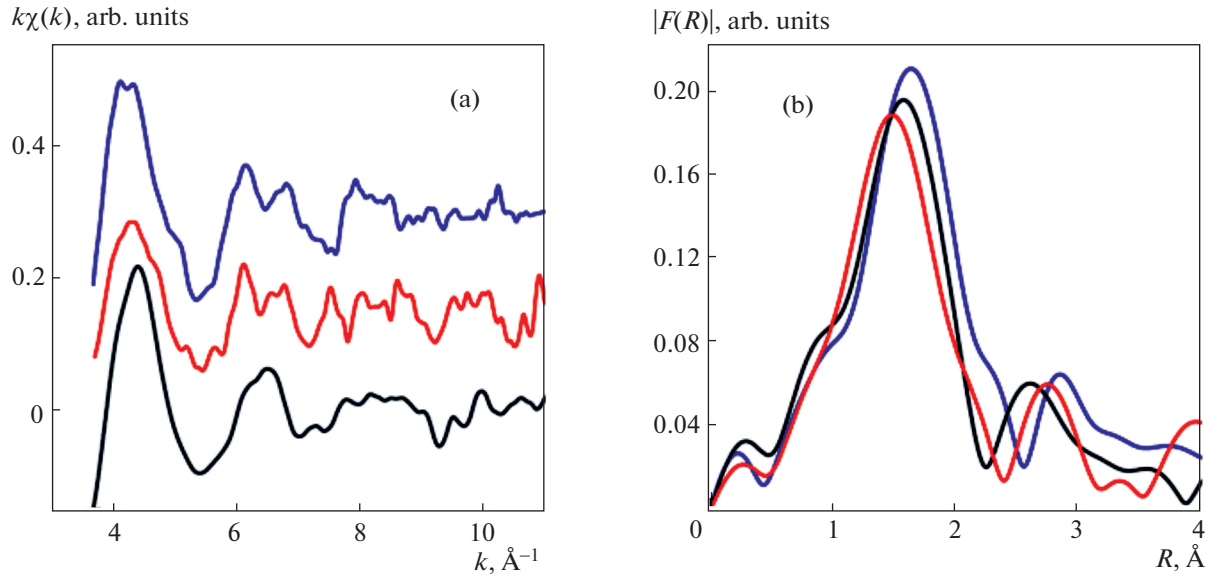
Fig. 2. (Color online) (a) Experimental ZrK EXAFS spectra and (b) moduli of their Fourier transform for films (black line) ZrO$_2$, (red line) amorphous Hf$_{0.5}$Zr$_{0.5}$O$_2$, and (blue line) polycrystalline Hf$_{0.5}$Zr$_{0.5}$O$_2$.

atoms in the shells were divided into groups with close interatomic distances. The average interatomic distances were then used for simulation. This division into groups seems to be useful to use data for starting models in simulating samples with a more complex composition. The results of simulating the reference HfO$_2$ and ZrO$_2$ oxides are given in Table 1.

4.1.2. Results of simulating the HfL_1 and ZrK EXAFS spectra of amorphous and polycrystalline Hf$_{0.5}$Zr$_{0.5}$O$_2$ films. As is seen from the XANES (X-ray absorption near-edge structure) spectra shown in Fig. 3, the energy position and the shape of the HfL_1 and ZrK absorption edges in Hf$_{0.5}$Zr$_{0.5}$O$_2$ almost coincide with the absorption edges of hafnium (HfO$_2$) and

Table 1. Parameters of the local Hf and Zr atom structure in the films: N is the coordination number, R is the interatomic distance, and σ^2 is the Debye–Waller factor (Fit is the fitting factor characterizing simulation quality, S_0^2 is the amplitude suppression factor). Fixed parameters are in bold type.

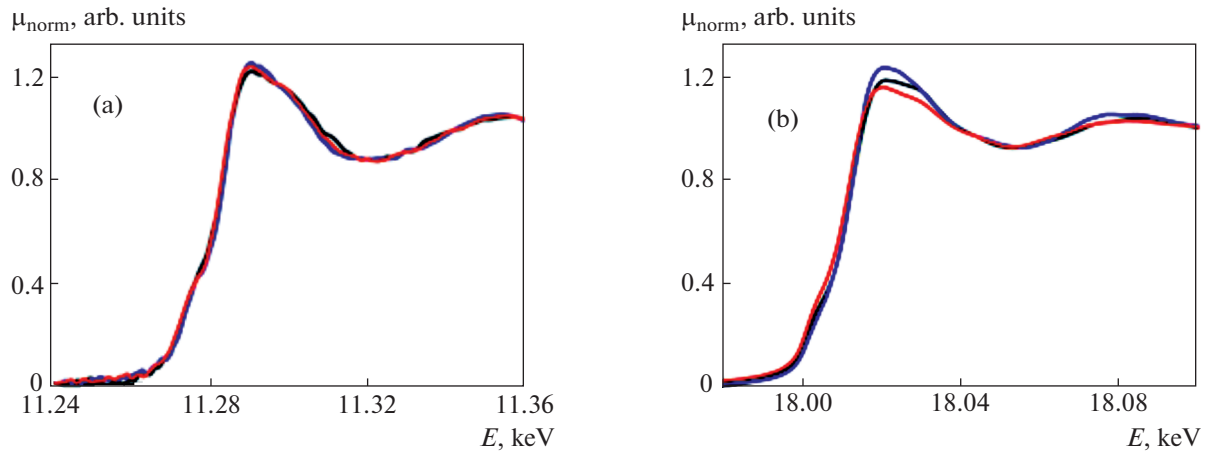| Sample	Absorbing atom– scattering atom	N	R, Å	σ^2, Å^2
HfO$_2$	Hf–O		2.13 ± 0.01	0.014 ± 0.001
	Hf–Hf		3.39 ± 0.03	0.019 ± 0
	Hf–O		3.50 ± 0.05	0.014
	Hf–Hf		4.06 ± 0.04	0.019
	Hf–O		4.23 ± 0.04	0.014
	Fit = 3.4, $S_0^2 = 0.9 \pm 0.1$			
ZrO$_2$	Zr–O		2.17 ± 0.01	0.012 ± 0.003
	Zr–Zr		3.34 ± 0.03	0.019 ± 0.005
	Zr–O		3.61 ± 0.05	0.012
	Zr–Zr		3.99 ± 0.04	0.019
	Zr–O		4.38 ± 0.04	0.012
	Fit = 5.1, $S_0^2 = 0.7 \pm 0.2$			

Fig. 3. (Color online) (a) Experimental XANES (a) HfL_1 and (b) ZrK spectra of films (red line) amorphous $Hf_{0.5}Zr_{0.5}O_2$, (blue line) polycrystalline $Hf_{0.5}Zr_{0.5}O_2$, and (black lines) reference HfO_2 and ZrO_2 oxides. μ_{norm} is the normalized X-ray absorption coefficient.
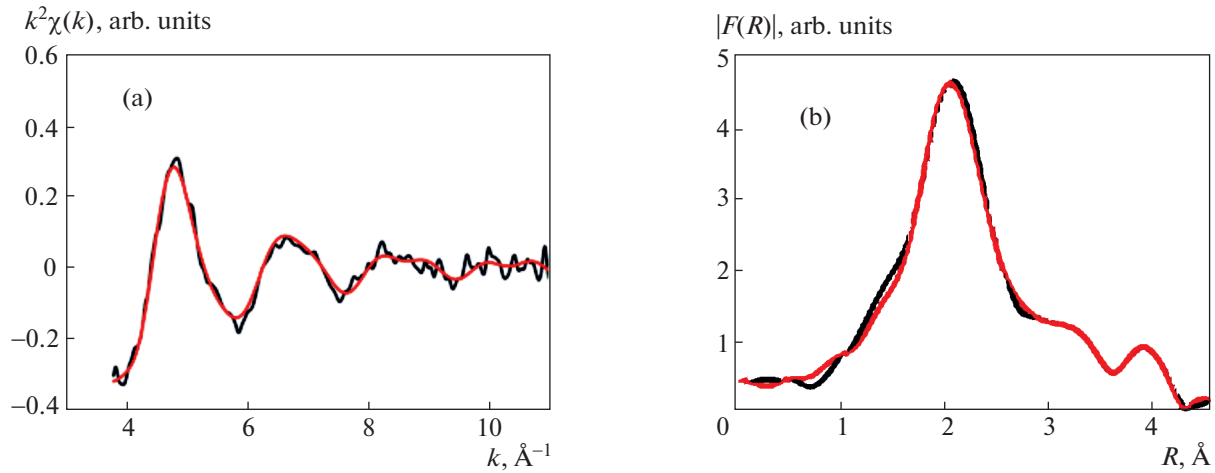

Fig. 4. (Color online) (black line) Experimental and (red line) simulated HfL_1 EXAFS spectra of (a) amorphous $Hf_{0.5}Zr_{0.5}O_2$ film and (b) moduli of their Fourier transform.

zirconium (ZrO_2) oxides. Therefore, we used the monoclinic structures of hafnium and zirconium oxides as the most probable ones at the given synthesis and annealing temperatures as initial models to calculate the spectra of the bimetallic oxides. It is known from the data in [19] and the structural database in [20], HfO_2 and ZrO_2 are full structural analogs. The zirconium and hafnium atoms in $Hf_{0.5}Zr_{0.5}O_2$ can substitute for each other, and the interatomic distances from one metal atom to two other metal atoms can be identical (file no. 2 106 614) [20].

Based on the structure of monoclinic HfO_2 (file no. 9 013 470) [18, 20], we can divide the metal atoms in far coordination shells into the following two groups with close interatomic distances: the first group consists of seven metal atoms with an average distance of

3.4 Å, and the second group consists of four metal atoms with an average distance of 3.9 Å. The total coordination numbers N for these shells are 7 and 4 ($N1$(Hf) + $N1$(Zr) = 7, $N2$(Hf) + $N2$(Zr) = 4), since both Hf and Zr atoms can exist at the same distance. According to the structural data [18], we introduced three oxygen shells with distances of 2.1, 3.8, and 4.2 Å into the calculation. The coordination numbers for the second and third oxygen shells are $N2$(O) = 5 and $N3$(O) = 11, respectively. The coordination number for the first coordination shell was calculated in simulation. The Hf–Hf and Hf–Zr distances were first the same and then "released" in calculation.

The model structure for fitting the ZrK spectrum was constructed similarly to the model of calculating the HfL_1 spectrum. Table 2 gives the data for simulat-

Table 2. Parameters of the local Hf atom structure in the amorphous and polycrystalline films and the Zr atom structure in the polycrystalline $Hf_{0.5}Zr_{0.5}O_2$ film. Fixed parameters are in bold type

Sample, line	Absorbing atom–scattering atom	N	R, Å	σ^2, Å^2
Amorphous film,	Hf–O	6.8 ± 1.3	2.12 ± 0.01	0.017 ± 0.001
	Hf–Hf	4.1 ± 1.0	3.22 ± 0.03	0.02 ± 0.01
	Hf–Zr	2.9	3.46 ± 0.02	
	Hf–O		3.31 ± 0.05	0.017
	Hf–Hf	2.5 ± 0.8	3.97 ± 0.04	0.02
	Hf–Zr	1.5	4.13 ± 0.02	
	Hf–O		4.17 ± 0.04	0.017
		Fit = 3.4, $S_0^2 = 0.9$		
Polycrystalline film, HfL_1	Hf–O	6.4 ± 1.5	2.14 ± 0.02	0.005 ± 0.001
	Hf–Hf	5.4 ± 1.0	3.35 ± 0.03	0.011 ± 0.00
	Hf–Zr	1.6	3.49 ± 0.02	
	Hf–O		3.35 ± 0.05	0.005
	Hf–Hf	3.1 ± 1.0	3.96 ± 0.04	0.011
	Hf–Zr	0.9	4.14 ± 0.02	
	Hf–O		4.22 ± 0.04	0.005
		Fit = 6.4, $S_0^2 = 0.9$		
Polycrystalline film, ZrK	Zr–O	6.5 ± 0.9	2.09 ± 0.02	0.016 ± 0.001
	Zr–Hf	2.1	3.46 ± 0.03	0.019 ± 0
	Zr–Zr	4.9 ± 1.2	3.50 ± 0.02	
	Zr–O		3.38 ± 0.05	0.016
	Zr–Hf	1.0	3.99 ± 0.04	0.019
	Zr–Zr	3.0 ± 0.8	3.94 ± 0.02	
	Zr–O		4.22 ± 0.04	0.016
		Fit = 4.5, $S_0^2 = 0.7$		

ing the HfL_1 and ZrK EXAFS spectra for the amorphous and polycrystalline films. In Figs. 4 and 5, we compare the simulated and experimental HfL_1 EXAFS spectra of the amorphous and polycrystalline $Hf_{0.5}Zr_{0.5}O_2$ oxide films.

It should be noted that the coordination numbers in the Hf–Hf and Hf–Zr coordination shells in the amorphous film are close to a ratio of 50/50 (with allowance for the accuracy of their determination). Thus, the amorphous $Hf_{0.5}Zr_{0.5}O_2$ film is assumed to consist of an "incompletely mixed" solid solution of the HfO_2 and ZrO_2 oxides.

In simulation pf the HfL_1 spectrum, the Debye factors of the polycrystalline sample are significantly lower than those of the amorphous sample. Therefore, after annealing, the metal oxides have a more ordered structure, which agrees with the appearance of a polycrystalline structure in this case [13]. An analysis of the obtained values of coordination number N showed that N(Hf–Hf) is larger than N(Hf–Zr) by a factor of 3–4 and N(Zr–Zr) is larger than N(Zr–Hf) by a factor of 2.5–3. Thus, after annealing, the hafnium and zirconium oxides are likely to form monoxide islands, which touch each other along interfaces, in the films. Although the experimental results do not allow us to determine the
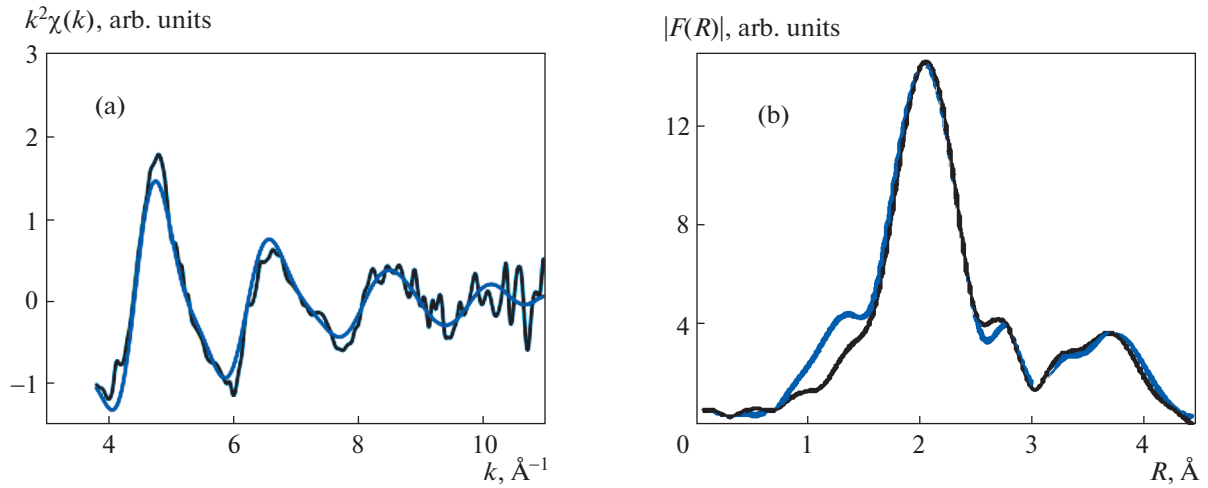
Fig. 5. (Color online) (black line) Experimental and (blue line) simulated HfL_1 EXAFS spectra of (a) polycrystalline $Hf_{0.5}Zr_{0.5}O_2$ film and (b) moduli of their Fourier transform.

sizes and the phase structure of the islands, we can assume that the HfO_2 and ZrO_2 island sizes are several nanometers and the island structure is analogous to the monoclinic structure of HfO_2 and ZrO_2.

4.2. Results Obtained from Ellipsometric Measurements

The spectral ellipsometric measurements of the $Hf_{0.5}Zr_{0.5}O_2/Si$ samples showed that these thin films were transparent in the spectral region under study and, hence, can be described by polynomial Cauchy relation (3) without regard for light absorption ($k = 0$). Table 3 gives the data calculated by the Cauchy model for all samples and the sample thicknesses.

To describe the multicomponent $Hf_{0.5}Zr_{0.5}O_2/Si$ film, we used the Bruggemann effective-medium model [15–17]. This model describes the complex optical medium as a mixture of ZrO_2 and HfO_2 phases, each of which has specific permittivity ε_i and

fraction q_i in the mixture. As the components that simulate the $Hf_{0.5}Zr_{0.5}O_2$ film composition, we took the amorphous HfO_2 and ZrO_2 films deposited by ion sputtering [21]. These results are shown in Figs. 6 and 7. Curves *1* and *3* in Fig. 7 reflect the dispersions of the ZrO_2 and HfO_2 films, respectively, and curve *2*, the dispersion of the $Hf_{0.5}Zr_{0.5}O_2$ film calculated by the polynomial Cauchy relation The dashed line illustrates the dispersion calculated by Bruggemann model (4), which is nearest to the experimental and calculated curves for the $Hf_{0.5}Zr_{0.5}O_2$ film (curve *2*). Table 3 presents the fractions of the Hf component in HfO_2 ($q = 0.46$ and 0.48 for the amorphous and polycrystalline films, respectively) for the best fitting of the calculated $\Psi(\lambda)$ and $\Delta(\lambda)$ curves to the experimental ones.

The low values of error function (functional) σ^2 indirectly indicate that the films are transparent, homogeneous (no thickness and refractive index gradients), and well correspond to the single-layer

Table 3. Thicknesses and optical characteristics of the films calculated by the Cauchy and Bruggemann models: d is the film thickness; n is the refractive index at a wavelength of 632.8 nm; a, b, and c are polynomial coefficients; σ^2 is the functional characterizing the accuracy of solving the inverse problem of ellipsometry; and q_{Hf} is the fraction of the Hf-containing component (HfO_2)

Sample	d, nm	n	Cauchy calculation			σ^2	q_{Hf}
			a	$b \times 10^{-4}$	$c \times 10^{-9}$		
HfO_2	88.9	2.003	1.955	1.834	0.264	1.21	−
ZrO_2	88.6	2.147	2.105	1.446	1.055	1.37	−
$Hf_{0.5}Zr_{0.5}O_2$ polycrystalline film	37.3	2.075	2.041	1.113	0.405	1.73	0.46
$Hf_{0.5}Zr_{0.5}O_2$ amorphous film	37.2	2.069	2.033	1.247	0.326	1.91	0.48
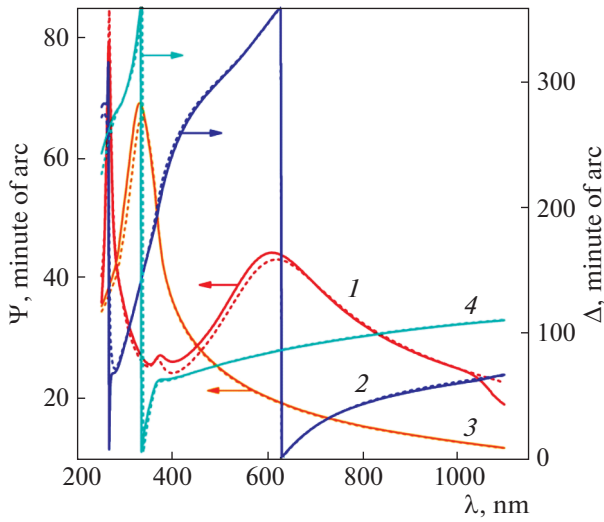
Fig. 6. (Color online) Ellipsometric angles (*1, 3*) Ψ and (*2, 4*) Δ vs. wavelength λ for (*1, 2*) HfO$_2$ and (*3, 4*) Hf$_{0.5}$Zr$_{0.5}$O$_2$/Si samples. (dashed lines) Cauchy fitting (see Table 3).

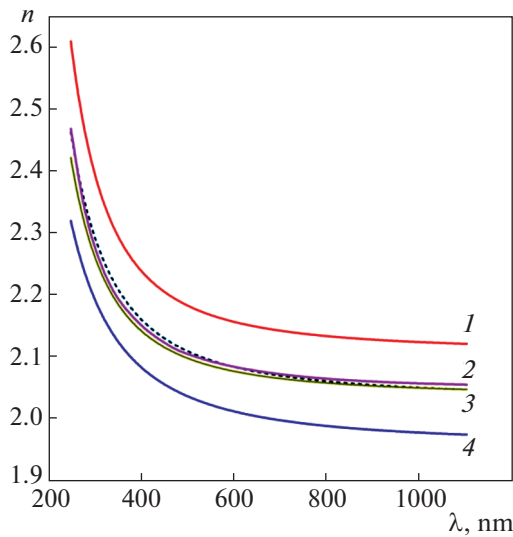**Fig. 7.** (Color online) Dispersion dependences $n(\lambda)$ for (*1*) ZrO$_2$ and (*2*) polycrystalline and (*3*) amorphous Hf$_{0.5}$Zr$_{0.5}$O$_2$ and (*4*) HfO$_2$ films. (dashed lines) Dependence $n(\lambda)$ calculated using curves *1* and *4* and the Bruggemann effective-medium model (q_{Hf} = 0.5).

reflecting system model (minimum of functional σ^2 characterizes the accuracy of solving the inverse problem of ellipsometry) [16].

5. CONCLUSIONS

As follows from the HfL_1 and ZrK EXAFS spectra, the metal atoms in amorphous and polycrystalline

Hf$_{0.5}$Zr$_{0.5}$O$_2$ films are coordinated by seven oxygen atoms (HfO$_7$ and ZrO$_7$, respectively). The EXAFS spectrum of the amorphous Hf$_{0.5}$Zr$_{0.5}$O$_2$ film demonstrates that it consists of an incompletely mixed solid solution of metallic oxides HfO$_2$ and ZrO$_2$. After RTA, the mixed Hf$_{0.5}$Zr$_{0.5}$O$_2$ oxide samples have a more ordered polycrystalline structure without the phase of mixed oxides and form Hf and Zr monoxide phase islands, which touch each other along interfaces. These islands are several nanometers in size and have a structure that is similar to the monoclinic structure of HfO$_2$ and ZrO$_2$. The HfO$_2$ and ZrO$_2$ phases were detected in the Hf$_{0.5}$Zr$_{0.5}$O$_2$ samples by ellipsometry.

REFERENCES

1. T. S. Böscke, J. Müller, D. Bräuhaus, U. Schröder, and U. Böttger, Appl. Phys. Lett. **99**, 102903 (2011).

2. S. Müller, J. Mueller, A. Singh, S. Riedel, J. Sundqvist, U. Schröder, and T. Mikolajick, Adv. Funct. Mater. **22**, 2412 (2012).

3. J. Müller, T. S. Böscke, U. Schröder, S. Mueller, D. Bräuhaus, U. Böttger, L. Frey, and T. Mikolajick, Nano Lett. **12**, 4318 (2012).

4. J. Müller, T. S. Böscke, D. Bräuhaus, U. Schröder, U. Böttger, J. Sundqvist, P. Kücher, T. Mikolajick, and L. Frey, Appl. Phys. Lett. **99**, 112901 (2011).

5. M. H. Park, H. J. Kim, Y. J. Kim, W. Lee, H. K. Kim, and C. S. Hwang, Appl. Phys. Lett. **102**, 112914 (2013).

6. M. H. Park, H. J. Kim, Y. J. Kim, W. Lee, T. Moon, and C. S. Hwang, Appl. Phys. Lett. **102**, 242905 (2013).

7. A. Chernikova, M. Kozodaev, A. Markeev, Yu. Matveev, D. Negrov, and O. Orlov, Microelectron. Eng. **147**, 15 (2015).

8. M. H. Park, Y. H. Lee, H. J. Kim, Y. J. Kim, T. Moon, K. D. Kim, J. Müller, A. Kersch, U. Schroeder, T. Mikolajick, and C. S. Hwang, Adv. Mater. **27**, 1811 (2015).

9. Crystallographic Space Group Symmetry Tables. univie.ac.at/nikos.pinotsis/spacegroup.html.

10. J. Wang, H. P. Li, and R. Stevens, J. Mater. Sci. **27**, 5397 (1992).

11. V. A. Gritsenko, J. B. Xu, I. H. Wilson, R. M. Kwok, Y. H. Ng, and I. H. Wilson, Phys. Rev. Lett. **81**, 1054 (1998).

12. V. A. Gritsenko, Phys. Usp. **51**, 699 (2008).

13. D. R. Islamov, A. G. Chernikova, M. G. Kozodaev, A. M. Markeev, T. V. Perevalov, V. A. Gritsenko, and O. M. Orlov, JETP Lett. **102**, 544 (2015).

14. N. Binsted, EXCURVE 98: CCLRC Daresbury Laboratory Computer Program (1998).

15. E. J. Rubio, V. V. Atuchin, V. N. Kruchinin, L. D. Pokrovsky, I. P. Prosvirin, and C. V. Ramana, J. Phys. Chem. C **118**, 13644 (2014).

16. *Handbook of Ellipsometry*, Ed. by H. G. Tompkins and E. A. Irene (William Andrew, New York, 2005).

17. S. Bosch, J. Ferré-Borrull, N. Leinfellner, and A. Canillas, Surf. Sci. **453**, 9 (2000).

18. R. Ruh and P. W. R. Corield, J. Am. Ceram. Soc. **53**, 126 (1970).

19. W. Zheng, K. H. Bowen, J. Li, I. Dabkowska, and M. Gutowski, J. Phys. Chem. A **109**, 11521 (2005).

20. Crystallography Open Database. www.crystallography.net.

21. V. S. Aliev, A. K. Gerasimova, V. N. Kruchinin, V. A. Gritsenko, I. P. Prosvirin, and I. A. Badmaeva, Mater. Res. Express **3**, 085008 (2016).

Translated by K. Shakhlevich